Improvement of EMI Filter Performance With Parasitic Coupling Cancellation

Shuo Wang, *Student Member, IEEE*, Fred. C. Lee, *Fellow, IEEE*, Willem Gerhardus Odendaal, *Member, IEEE*, and Jacobus Daniel van Wyk, *Fellow, IEEE*

***Abstract*—In this paper, critical parasitic couplings in EMI filters are first identified. Based on the understanding of filter parasitics, methods are proposed to improve EMI filter performance by canceling critical couplings. A cancellation inductor is then integrated with capacitors to cancel the mutual coupling between two capacitors and the equivalent series inductance (ESL) of the integrated capacitor. The proposed method is applied to both rectangular and tubular capacitors. Two different integration approaches are also compared. Finally, prototypes are built and tested for both one-stage and two-stage EMI filters. Experimental results show the proposed mutual coupling cancellation technique can drastically improve EMI filter high frequency performance.**

***Index Terms*—Electromagnetic interference (EMI) filter, equivalent series inductance (ESL), integrated capacitor with cancellation inductor, mutual coupling cancellation, parasitic coupling.**

I. Introduction

PARASITIC parameters affect electromagnetic interference (EMI) filter performance significantly in the high frequency (HF) range. Generally, there are two types of parasitic parameters: self-parasitics and mutual parasitics. The self-parasitics include the equivalent series inductance (ESL) and equivalent series resistance (ESR) of capacitors, equivalent parallel capacitance (EPC) and equivalent parallel resistance (EPR) of inductors. The mutual parasitics exist between two components, between a component and the printed circuit board (PCB) layout and between PCB traces. For the differential mode (DM) EMI filter shown in Fig. 1, the circuit model including all these parasitics had been built in [1] and [3] and is shown in Fig. 2.

In Fig. 2, the ESR1, 2 and ESL1, 2 are the self-parasitics of the two capacitors. EPC and EPR are the self-parasitics of the inductor. L_{p1} and L_{p2} are the self-inductances of the input and output trace loops. The mutual parasitics can be divided into five categories as follows.

1) Coupling between inductor and capacitors: M_1 and M_2.
2) Coupling between two capacitors: M_3.
3) Coupling between inductor and trace loops: M_4 and M_5.
4) Coupling between ground plane and inductor: M_7 and C_p.
5) Coupling between trace loops: M_6.

Manuscript received September 9, 2004; revised December 14, 2004. This work was supported by the Engineering Research Center Program of the National Science Foundation under NSF Award EEC-9731677. Recommended by Associate Editor F. Blaabjerg.

The authors are with the Bradley Department of Electrical and Computer Engineering, Virginia Polytechnic Institute and State University, Blacksburg, VA 24061 USA (e-mail: shwang6@vt.edu).

Digital Object Identifier 10.1109/TPEL.2005.854069

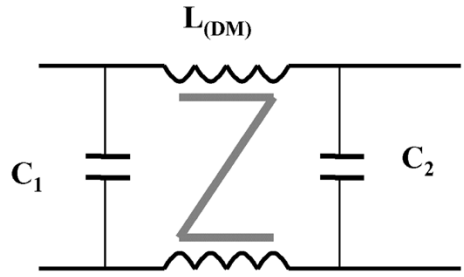

Fig. 1. Investigated one-stage DM EMI filter.

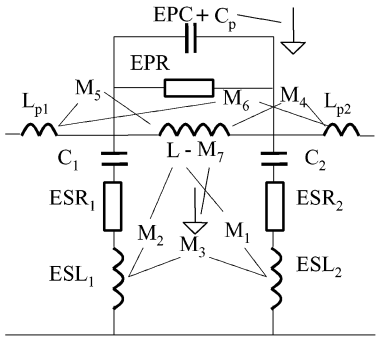

Fig. 2. Parasitic model for a one-stage EMI filter.

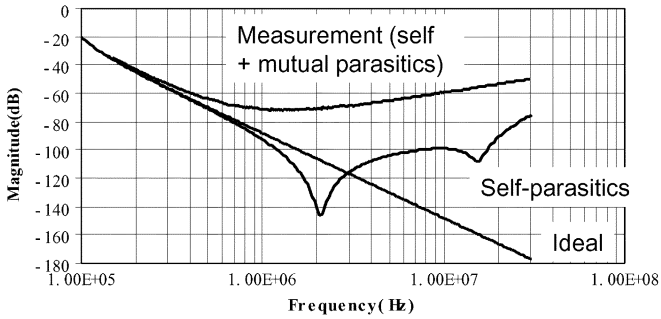

Fig. 3. Effects of parasitic parameters on EMI filter performance (Insertion voltage gain when both source and load are 50 Ω).

The effects of parasitic parameters on EMI filter performance are illustrated in Fig. 3. In Fig. 3, three insertion voltage gains with 50 Ω source and load impedances are compared by simulation, where insertion voltage gain is defined as the ratio of the port voltage at the load side without the filter to that with the filter. The self-parasitics curve is the simulation result of the filter model including only the self-parasitics. Obviously, in the HF range, the self-parasitics make EMI filter performance worse than the ideal case; however the measured curve shows that the mutual parasitics finally determine the EMI filter HF

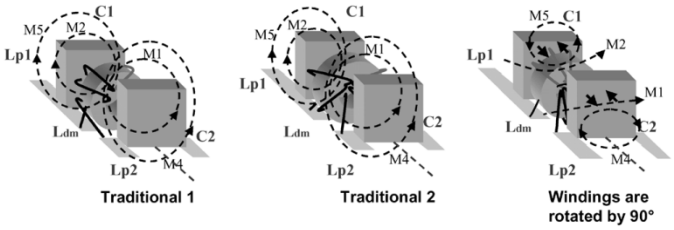

Fig. 4. Rotating inductor windings by 90° to reduce mutual inductance M_1, M_2, M_4, and M_5.

performance. Based on this comparison, EMI filter performance can be significantly improved by controlling parasitic couplings.

Reference [5] introduced a network method to cancel the ESL of capacitors. References [7] and [8] employed mutual inductance to cancel the ESL of capacitors. All of these methods are for the reduction of self-parasitics. Since EMI filter is a coupled system, reduction of mutual parasitics is even more important than the reduction of self-parasitics. In fact, experiments show that if mutual couplings are not efficiently minimized, efforts on reducing self-parasitics could be in vain. Before these methods can be effectively applied to filter design, effects of mutual couplings must be minimized. Reference [2] shielded two capacitors and enlarged the distance between components to reduce the couplings, but this was at the cost of larger size and extra parasitics. In [1] and [2], inductor windings were rotated by 90° to make magnetic flux symmetrical to the center line of capacitors and trace loops. As shown in Fig. 4, after windings are rotated by 90°, the net magnetic flux linking capacitors C_1, C_2 and trace loops L_{p1}, L_{p2} are greatly reduced so that mutual inductances M_1, M_2, M_4, and M_5 can be reduced by more than 90%. The improvement of these two methods on filter performance is still limited [1], [2]. In order to significantly improve EMI filter performance, critical parasitic couplings must be identified and greatly reduced.

The effect of mutual inductance M_1 on capacitor C_2 is equivalent to an inductance M_1 in series with the ESL of capacitor C_2 [1]. The same rule holds true for the effect of M_2 on C_1. Because M_1 and M_2 can be several times larger than the ESL of the capacitors [1], they are critical to the capacitor performance. The effect of M_4 or M_5 can also be equivalent to an inductance in series with the ESL of the capacitors; however they are not critical because they are much smaller than M_1 and M_2. Due to the large magnitude difference between the HF currents on the branches C_1 and C_2, the effect of M_3 on capacitor performance is significant [1]. The mutual inductance M_6 between input and output trace loops also plays an important role in filter performance for the same reason [1]. For M_7 and C_p, they are not critical to filter performance [1].

Experiments in [1] showed that, in HF range, after the inductor windings are rotated by 90°, effects of M_1 and M_2 on filter performance are greatly reduced. As a result, effects of M_3 and M_6 are significant so that the insertion voltage gain of the filter is given by (1). This can be explained by the high impedance of the inductor actually causing noise to propagate to the load through the mutual couplings between the two capacitors and between the input and output trace loops. In order to further improve the EMI filter HF performance, M_3 and M_6 should be minimized. M_6 can be easily minimized by minimizing the input and output trace loop areas. For M_3, this paper introduces

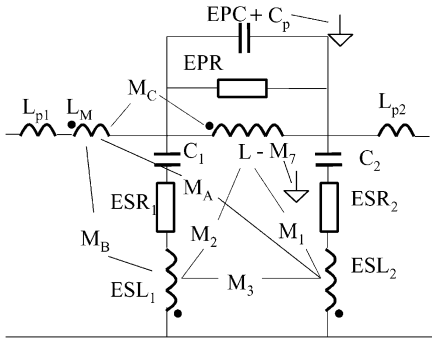

Fig. 5. EMI filter model with a cancellation inductor L_M.

a new technique to effectively cancel it and consequently drastically improve filter HF performance

$$\mathbf{T_G} = \frac{2\mathbf{U_2}}{\mathbf{U_S}} \approx \frac{j\omega}{25}(M_3 + M_6). \tag{1}$$

II. Parasitic Coupling Cancellation

In this paper, a cancellation turn is integrated with the capacitors to cancel the parasitic coupling between the two capacitors. Two approaches are investigated. For the first approach, a cancellation turn is in series with the input or output trace loop. For the second approach, a cancellation turn is in series with either capacitor C_1 or C_2. It can be shown that for the first approach, the integrated cancellation turn can reduce both the coupling between two capacitors and the ESL of the capacitor. Two measures are firstly taken before applying these two approaches to the filter.

1) Input and output trace loops are reduced as much as possible to minimize mutual inductance M_4, M_5, and M_6.
2) Inductor windings are rotated by 90° to reduce mutual inductance M_1, M_2, M_4, and M_5.

With the help of these two measures, the effects of M_4, M_5, and M_6 are greatly reduced. Because the current loop areas in the capacitors cannot be reduced, experiments show M_1 and M_2 are still 7.5 nH [1] and cannot be ignored in comparison with 14 nH ESL. M_3 is the same as the original, because no measure has been taken to reduce the coupling loop areas of two capacitors.

A. First Approach

In Fig. 5, a cancellation inductor L_M is introduced in series with the input trace loop. It has mutual inductance M_A with capacitor C_2, M_B with capacitor C_1 and M_C with inductor L. As analyzed in Section I, in HF range current does not flow through the inductor L, so the corresponding HF model of the filter is simplified as in Fig. 6. The effects of M_1, M_2, and M_C are ignored since no HF current flows through the inductor. The equivalent HF model with a load Z_L and input voltage $\mathbf{V_S}$ is shown in Fig. 7.

The load voltage $\mathbf{V_L}$ is then given as (2) shown at the bottom of the next page. Obviously, the condition for zero load voltage is given by

$$M_A = M_3. \tag{3}$$

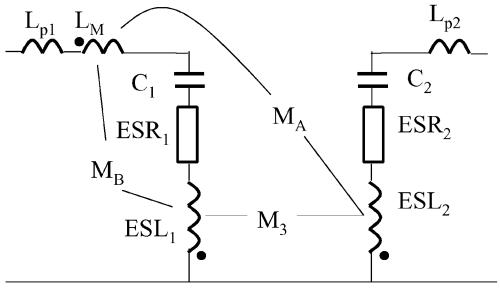

Fig. 6. HF model of the filter.

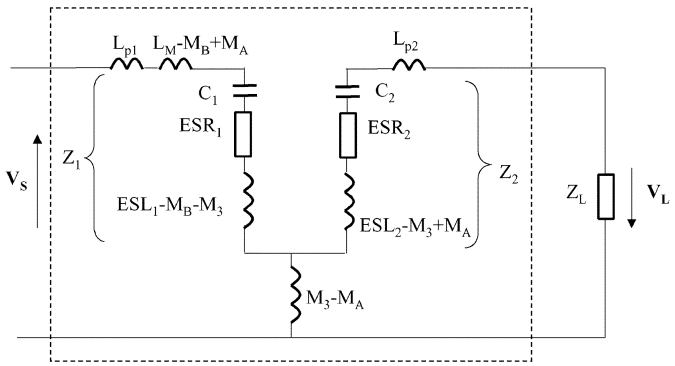

Fig. 7. HF equivalent circuit for the filter.

This condition means the mutual inductance between the cancellation inductor L_M and the capacitor C_2 should be equal to that between two capacitors. Furthermore, these two mutual couplings should have opposite polarities to obtain the desired cancellation effect just as shown in Fig. 5. The physical effect of the cancellation is that the induced voltage in C_2, due to the coupling between the cancellation inductor L_M and C_2, cancels the induced voltage due to the coupling between the two capacitors, because of opposite voltage directions. It should be pointed out that if M_A is much larger than M_3, a large equivalent negative inductance can be detrimental to filter performance. The proposed approach differs from the existing self-parasitic cancellation methods in that the critical mutual couplings are cancelled based on the understanding of the whole filter. As a result, the HF performance of the whole filter rather than a single component in the filter can be significantly improved.

After M_3 is cancelled, HF noise will propagate through the inductor. As a result, the effects of M_1, M_2, and ESL can become important. As stated in Section I, after the inductor windings are rotated by 90°, M_1 and M_2 have been reduced by more than 90%. After introducing inductor L_M, the effects of M_2 can be further reduced because of the cancellation effects of induced voltages in C_1. Another benefit of this approach is that the ESL of C_1 can be partly cancelled. Fig. 8 shows the equivalent circuit of C_1, which illustrates these two benefits. This equivalent circuit including M_B and M_C is different from that in Fig. 7 because HF noise propagates through the inductor after M_3 is

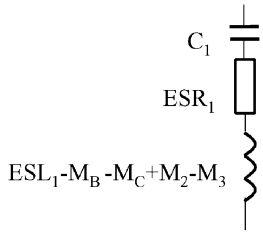

Fig. 8. Equivalent circuit for capacitor C_1.

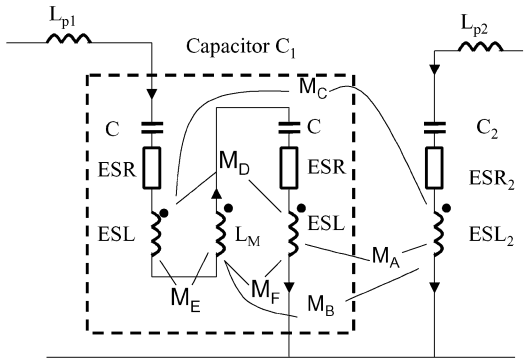

Fig. 9. HF model of the filter.

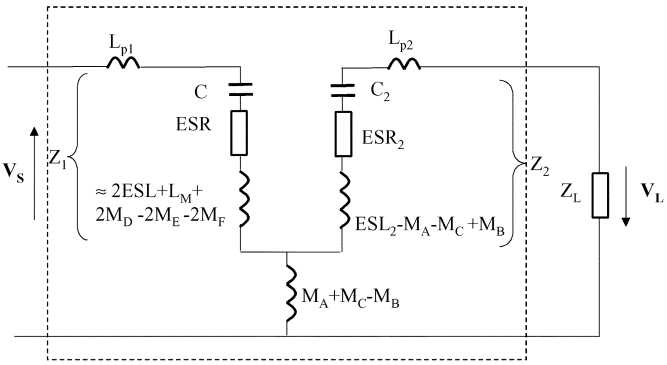

Fig. 10. HF equivalent circuit for the filter.

cancelled. In Fig. 8, if M_B and M_C makes the equivalent inductance smaller than ESL_1, the performance of capacitor C_1 is improved.

B. Second Approach

In the second approach, the capacitor C_1 is split into two identical parts. As shown in Fig. 9, the cancellation turn L_M is in series with the two split capacitors at the middle point. All the mutual inductances between any two components are shown in Fig. 9. The HF equivalent circuit is shown in Fig. 10. In Fig. 10, if $M_A + M_C = M_B$ (the mutual inductance between the split capacitors and C_2 should equal the mutual inductance between the cancellation turn and C_2), then the output of the filter is zero. However, the equivalent series inductance of the integrated structure can be enlarged, because the inductance L_M of the cancellation turn can be larger than the sum of $2M_E$ and $2M_F$. The couplings between the cancellation turn and capacitors should

$$\mathbf{V_L} = \frac{j\omega(M_3 - M_A)Z_L}{j\omega(M_3 - M_A)(Z_2 + Z_L) + Z_1(Z_2 + Z_L + j\omega(M_3 - M_A))}\mathbf{V_S} \tag{2}$$

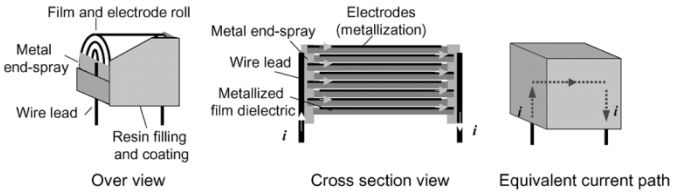

Fig. 11. Internal structure and current flow of film capacitors.

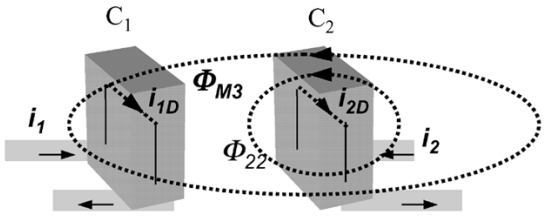

Fig. 12. Mutual coupling between two capacitors.

have the same polarities as those shown in Fig. 9. The advantage of this approach is that, the integrated capacitor is a two-terminal component and the structure is symmetrical, which may benefit manufacturing.

III. Implementation

A. Internal Structure of Film Capacitors

The commonly used dielectrics for DM EMI capacitors are metallized film and paper. The commonly used capacitor shapes are rectangular and tubular. The general internal structure of a rectangular film capacitor is shown in Fig. 11 [10]. Electrodes are metallized on one side of the plastic film. Two layers of films are stacked and rolled together. The roll is then embedded in resin filling and plastic coating. The ends are metal-sprayed and wire leads are soldered on the two sides of the roll to conduct the current. The film acts as the dielectric of the capacitor. The current flow in the capacitor is also illustrated in Fig. 11.

In Fig. 11, the current is first conducted through the wire lead and metal end-spray on one end of the roll. It then goes through the electrodes and film dielectric. Finally, the current reaches the wire lead and metal end-spray on the other end of the roll. The electrodes and film dielectric therefore form a capacitor. Obviously, there is a current loop in the capacitor. It is this current loop that links the external magnetic flux so as to generate mutual inductance. This rule also holds true for capacitors in other shapes.

B. First Approach

Based on the analysis in Section II, the mutual inductance $\mathrm{M_A}$ between the cancellation inductor $\mathrm{L_M}$ and capacitor $\mathrm{C_2}$ should equal the mutual inductance $\mathrm{M_3}$ between $\mathrm{C_1}$ and $\mathrm{C_2}$. The magnetic coupling between $\mathrm{C_1}$ and $\mathrm{C_2}$ is illustrated in Fig. 12.

In Fig. 12, the magnetic flux Φ_{M3} produced by the current i_2 in capacitor $\mathrm{C_2}$ links the current i_1 in capacitor $\mathrm{C_1}$. The mutual inductance $\mathrm{M_3}$ is defined by (4). It should be pointed out that the current in the capacitor dielectric is displacement current (i_{1D}, i_{2D})

$$M_3 = \frac{\Phi_{M3}}{i_2}. \tag{4}$$

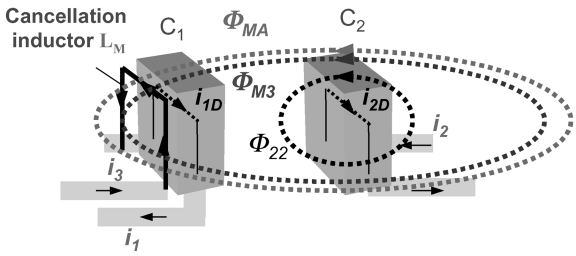

Fig. 13. Mutual coupling between two capacitors and between $\mathrm{C_2}$ and the cancellation turn.

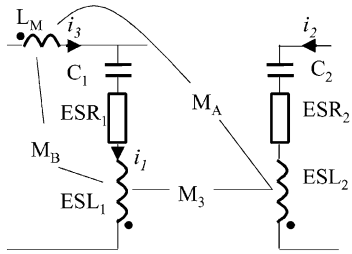

Fig. 14. Equivalent circuit of two capacitors when one is with a cancellation turn.

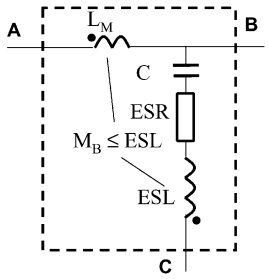

Fig. 15. Equivalent circuit of the integrated capacitor.

In Fig. 13, a cancellation inductor is added beside $\mathrm{C_1}$, where the cancellation inductor is a $3/4$ turn, which has a similar current path as the capacitor. If Φ_{MA} is the magnetic flux produced by $\mathrm{C_2}$ which links the cancellation inductor $\mathrm{L_M}$, the mutual inductance $\mathrm{M_A}$ between $\mathrm{L_M}$ and $\mathrm{C_2}$ is then given by

$$\mathrm{M_A} = \frac{\Phi_{\mathrm{MA}}}{i_2}. \tag{5}$$

Comparing (4) and (5), it is obvious that only when Φ_{MA} equals Φ_{M3} will $\mathrm{M_A}$ equal $\mathrm{M_3}$. It is difficult to theoretically calculate the coupling area of the cancellation turn because of the complicated magnetic flux distribution. However, the optimal coupling area of the cancellation turn can be tuned by conducting experiments. In order to efficiently cancel $\mathrm{M_3}$, the cancellation turn should also be close to capacitor $\mathrm{C_1}$ so as to be exposed to a similar external magnetic flux distribution to that of $\mathrm{C_1}$. A good way to do this is to integrate the cancellation inductor with the capacitor. Fig. 14 is the equivalent circuit of Fig. 13.

Since commonly used capacitors are rectangular and tubular, a cancellation turn will be applied to both shapes in this section. Fig. 15 shows the equivalent circuit of the integrated capacitor, where a cancellation inductor $\mathrm{L_M}$ is integrated with the capacitor. The mutual couplings between the integrated elements and

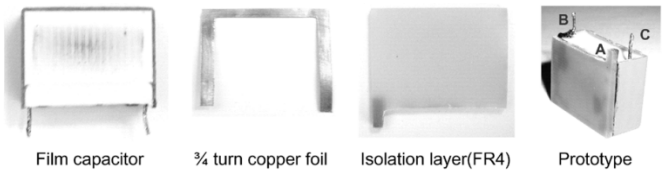

Fig. 16. Exploded view of the capacitor with an integrated cancellation turn.

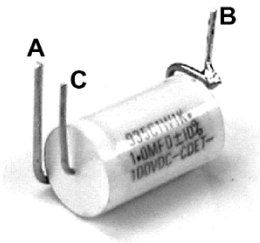

Fig. 17. Prototype of the integrated tubular film capacitor.

external components are not shown in the figure. In this implementation, a cancellation turn, which is composed of 3/4 turn of copper foil, is integrated in the film capacitor (Philips, MKP 0.47 μF/400 V). An isolation layer (FR4) covers the integrated cancellation turn. Fig. 16 shows the exploded view of the prototype. The three terminals in Fig. 16 correspond to those in Fig. 15.

In order to effectively cancel M_3, three measures are taken in the design of the cancellation turn.

1) The plastic coating of the capacitor is removed and the cancellation turn is glued as close as possible to the film roll of the capacitor. This guarantees the cancellation turn is exposed to a similar external magnetic field distribution to the capacitor.
2) The cancellation turn covers the side and upper edges of the film roll, so most of the flux that links the capacitor also links the cancellation turn.
3) Because the HF current always flows through the inner edge of the copper foil turn, the coupling area of the cancellation turn is determined by the area enclosed by the inner edge. The optimal area is tuned by conducting experiments.

A prototype for a tubular shape film capacitor was also built and is shown in Fig. 17. The cancellation turn is 3/4 turn wire and the capacitance is 1 μF.

C. Second Approach

For the second approach, the equivalent circuit and structure of the integrated capacitor are shown in Fig. 18. In the experiment, two 0.39-μF film capacitors (Cap1 and Cap2 in Fig. 18) and 3/4 turn copper foil are used for integration. The design of the cancellation turn is similar to that in the first approach.

IV. Experimental Results

In this section, the prototypes are tested both in one-stage and two-stage EMI filters. For the first approach, both rectangular and tubular capacitor prototypes are measured. The two integration approaches are also compared through experiments. The cancellation of mutual couplings and ESL are then quantified through the developed parasitic-extraction techniques [3].

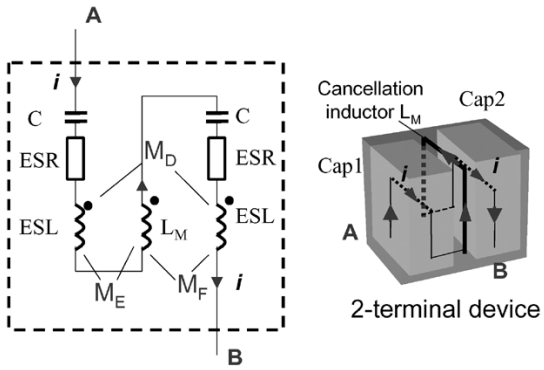

Fig. 18. Equivalent circuit and structure of the integrated capacitor.

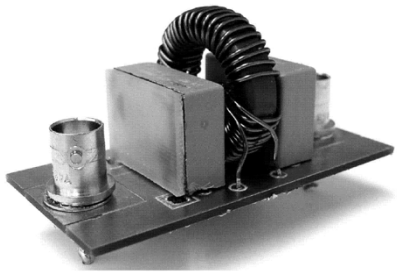

Fig. 19. One-stage EMI filter using the capacitor with an integrated cancellation turn.

Comparison of the measured results with the base line shows the drastic performance improvement on filter HF performance.

A. Application to a One-Stage EMI Filter

In the experiment, the inductance of the filter inductor is around 20 μH. The two measures proposed in Section II to reduce $\mathrm{M}_1, \mathrm{M}_2, \mathrm{M}_4, \mathrm{M}_5$, and M_6 are first applied to the investigated EMI filter.

For the first approach, the prototype of the rectangular capacitor replaced C_1 in the filter, as shown in Fig. 19. The comparative experimental results are shown in Figs. 20–22. All of the mutual inductances are extracted using the developed S-parameters method [3]. Fig. 20 shows the impedances of M_3 with and without cancellation. The noise below 1 mΩ is the result of the noise floor of the network analyzer.

Comparing the impedances above 1 mΩ, inductance M_3 is reduced from 249 pH to 19 pH which is a 92.4% reduction. Fig. 21 shows the impedance of capacitor C_1 with and without cancellation. From the change of the series resonant frequency of the capacitor, it is easy to derive that ESL of the integrated capacitor is reduced from 12 nH to 4 nH which is a 67% reduction because C1 is known as 0.486 μF. The performance of the filter is shown in Fig. 22. Three curves are compared. The base line case is the insertion voltage gain without using mutual coupling cancellation and 90° rotated windings. When the inductor windings are rotated by 90°, the filter has about 5 dB improvement, as shown by the second curve. The final case is the insertion voltage gain of the filter with 90° rotated windings and mutual coupling cancellation. The insertion voltage gain is indeed below the noise floor of the network analyzer above 1 MHz. The cancellation of M_3 and the ESL of capacitor C_1 results in a factor of 100 improvement (40 dB) in filtering performance at 30 MHz. The noise in Fig. 22 is the noise floor of the network analyzer.

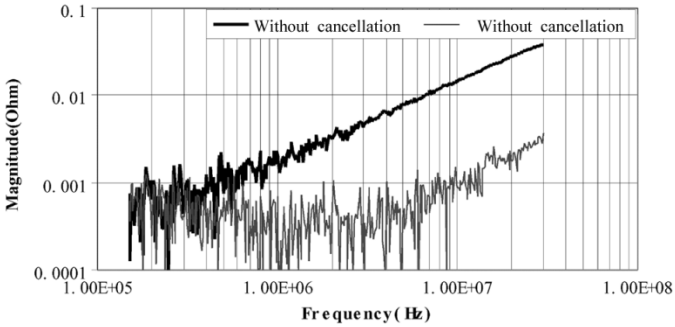

Fig. 20. Comparison of impedances of the mutual inductances between two capacitors.

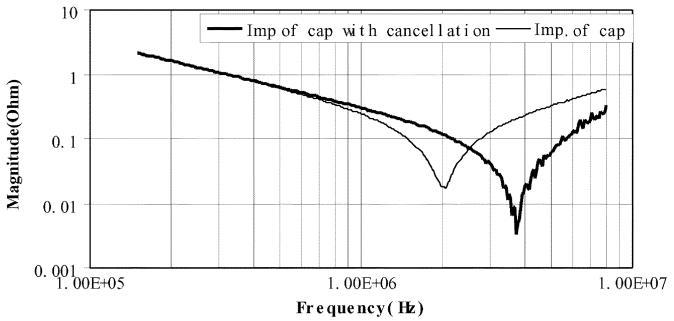

Fig. 21. Comparison of impedances of capacitor C_1.

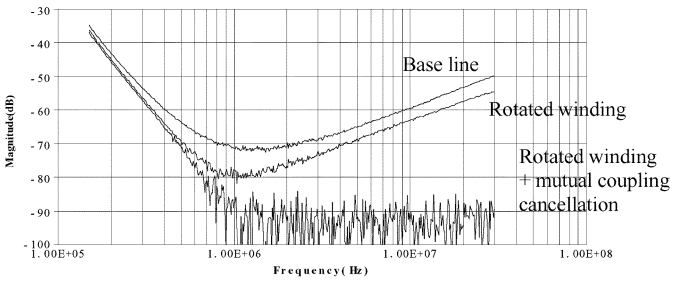

Fig. 22. Comparison of insertion voltage gains of a filter with and without mutual coupling cancellation for rectangular capacitors.

For the prototype of the tubular film capacitor, the measured filter has the same structure as that in Fig. 19 except that two capacitors are tubular shapes and the capacitance is 1 μF. The measured three insertion voltage gains are shown in Fig. 23. From Fig. 23, the filter with an integrated capacitor achieves 20 dB improvement at 30 MHz compared with the base line. Based on the results of these two experiments, it can be concluded that the proposed method can be used for both rectangular and tubular capacitors.

For the second approach, the measured filter has the same structure as that in Fig. 19, except that the equivalent capacitance for C_1 is 0.195 μF and C2 is 0.39 μF. The measured two insertion voltage gains are shown in Fig. 24. From Fig. 24, the filter with an integrated capacitor achieves ≤ -90 dB from 1 MHz to 13 MHz. The improvement above 13 MHz is still significant although it is not as good as the first approach due to enlarged ESL on C_1. This also verified that the mutual inductance between two capacitors is more important than the self-parasitics. Because the first approach has the better filtering performance, it is preferred in this paper.

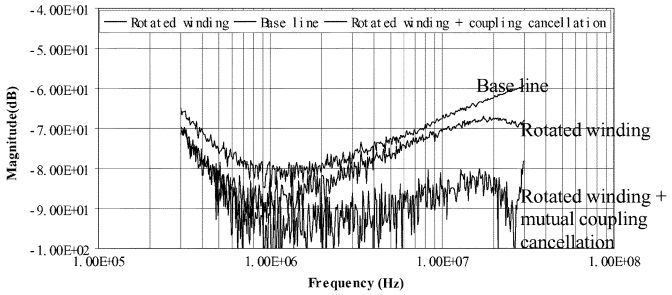

Fig. 23. Comparison of insertion voltage gains of a filter with and without mutual coupling cancellation for tubular capacitors.

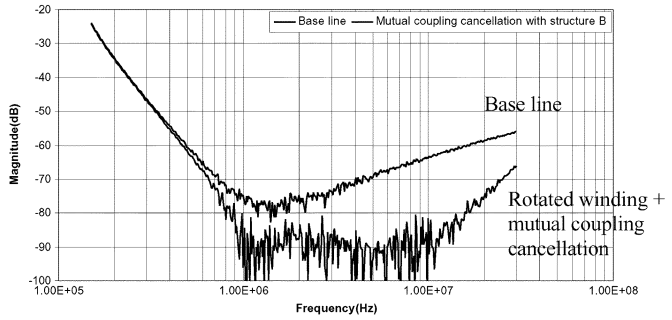

Fig. 24. Comparison of insertion voltage gains of a filter with and without mutual coupling cancellation for the second approach.

B. Application to a Two-Stage EMI Filter

The prototype of the rectangular capacitor in the first approach is also applied to a two-stage EMI filter. The filter circuit is shown in Fig. 25. The parasitic model is shown in Fig. 26 [3]. In the model, the mutual inductances between the input/output trace loop and other components are ignored because the trace loop area is kept very small. The mutual inductance M_9 between C_1 and C_3 are very critical to filter HF performance for the same reason they are critical in the one-stage EMI filter, which can be illustrated by the comparative experiments in Fig. 27. In Fig. 27, the base-line case is the insertion voltage gain of a two-stage EMI filter. The second curve is the insertion voltage gain of the filter when L_1, L_2, and C_2 are disconnected from the filter. Obviously, above 400 kHz, these two cases are almost the same, so the filter performance is almost determined by the inductive coupling between C_1 and C_3 above 400 kHz. M_1, M_2, M_3, and M_4 are the mutual inductances between inductors and capacitors. They also affect filter performance because of their effects on capacitors. The gain dip around 200 kHz in the base-line case is strongly affected by the mutual inductance M_{10} between two inductors [3]. This mutual inductance together with M_2, M_3 resonates with C_2 so as to cause an impedance dip and therefore a gain dip at the resonant frequency. However, this gain dip is desired because high attenuation is needed in the low frequency range to attenuate switching noise. Based on these analyses, two measures are taken to improve two-stage EMI filter performance.

1) Capacitor C_1 is replaced by the integrated capacitor prototype (rectangular shape) to reduce M_9.
2) The inductor windings are rotated by 90° to reduce M_1, M_2, M_3, and M_4.

After these two measures are taken, the results of experiments show the mutual inductance between C_1 and C_3 is reduced from

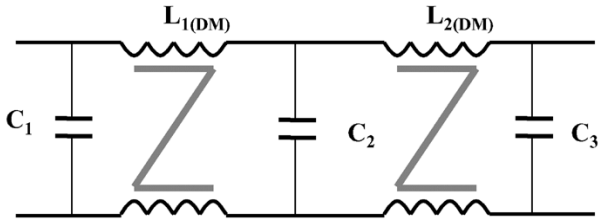

Fig. 25. Investigated two-stage DM EMI filter.

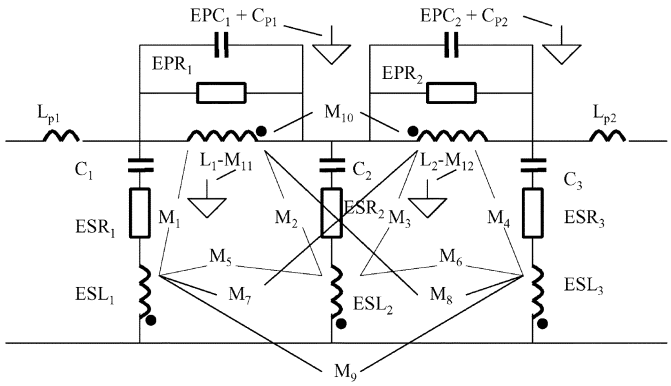

Fig. 26. Parasitic model for a two-stage DM EMI filter.

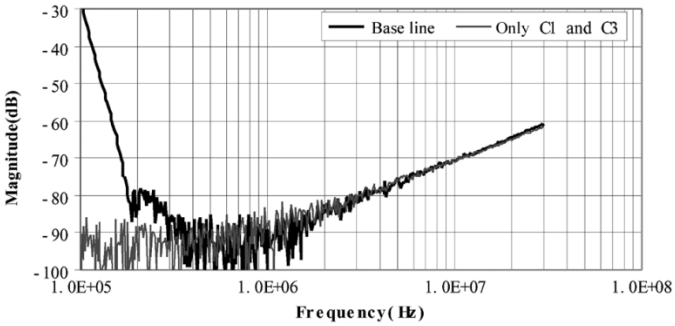

Fig. 27. Comparison of insertion voltage gains.

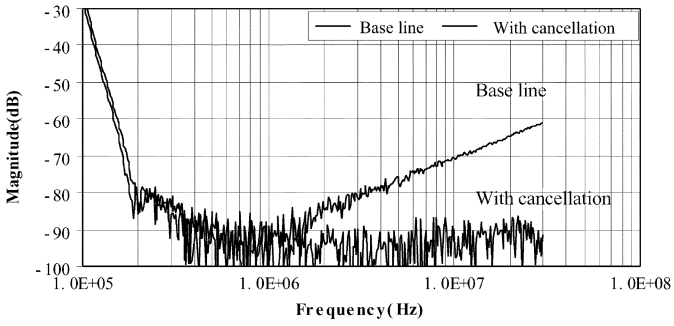

Fig. 28. Comparison of insertion voltage gains of a two-stage EMI filter with and without mutual coupling cancellation.

110 pH to 14 pH which is an 87.3% reduction. The ESL reduction is the same as in the one-stage filter case. Fig. 28 shows a comparison of the filter performance. The base-line case is the insertion voltage gain of the filter without using 90° rotated windings and mutual coupling cancellation. The second curve shows the filter performance with the 90° rotated windings and mutual coupling cancellation.

In Fig. 28, the measured insertion voltage gain is actually lower than the noise floor (−90 dB) of the network analyzer above 400 kHz, which implies a very good HF filtering performance. Compared with the base line, the performance after using the mutual coupling cancellation is improved from −60 dB to below −90 dB. More than 30 dB improvement is achieved at 30 MHz. Although the cancellation turn can also cancel M_1 and M_5, it is not as important as the cancellation of M_9.

It should be pointed out that because the cancellation turn already cancels M_9, only one of the two capacitors is needed to be replaced by the integrated capacitor on the two sides of the filter. For the electromagnetic interference from the outside of the filter, it is also expected that the cancellation turn can at least partly cancel these effects on the capacitors because of the opposite coupling polarities between the capacitor and the cancellation turn.

V. Conclusion

This work first identified the critical mutual couplings in EMI filters. These critical couplings are the mutual inductances between the input and output capacitors, between capacitors and inductors and between input and output trace loops. The latter two critical couplings can be overcome by rotating inductor windings by 90° and minimizing input/output trace loops. A cancellation inductor is proposed in this paper to cancel the mutual inductance between the two capacitors. This cancellation inductor can also partly cancel the ESL of the capacitors. A cancellation turn working as the cancellation inductor is then integrated into a capacitor. Two different integration approaches are investigated and compared. Prototypes are finally tested in both one-stage and two-stage EMI filters. Experiments show that the proposed method works well for both rectangular and tubular film capacitors. The cancellation effects of the cancellation turn on the mutual inductance between the input and output capacitors and on the ESL of a capacitor are quantified through experiments. The measurements show the cancellation approach can achieve <-90 dB improvement in filtering performance above 1 MHz for one-stage filters and the same above 400 kHz for two-stage EMI filters.

References

[1] S. Wang, F. C. Lee, D. Y. Chen, and W. G. Odendaal, "Effects of parasitic parameters on EMI filter performance," *IEEE Trans. Power Electron.*, vol. 19, no. 3, pp. 869–877, May 2004.

[2] S. Wang, F. C. Lee, and W. G. Odendaal, "Controlling the parasitic parameters to improve EMI filter performance," in *Proc. IEEE Applied Power Electronics Conf.*, vol. 1, Anaheim, CA, Feb. 22–26, 2004, pp. 503–509.

[3] S. Wang, W. G. Odendaal, and F. C. Lee, "Extraction of parasitic parameters of EMI filters using scattering parameters," in *Proc. IEEE Industry Applications Soc. Annu. Meeting*, vol. 4, Seattle, WA, Oct. 3–7, 2004, pp. 2672–2678.

[4] S. Wang, F. C. Lee, and W. G. Odendaal, "Using scattering parameters to characterize EMI filters," in *Proc. IEEE Power Electronics Specialists Conf.*, Aachen, Germany, June 20–25, 2004, pp. 297–303.

[5] ——, "Using a network method to reduce the parasitic parameters of capacitors," in *Proc. IEEE Power Electronics Specialists Conf.*, Aachen, Germany, Jun. 20–25, 2004, pp. 304–308.

[6] R. Chen, J. D. van Wyk, S. Wang, and W. G. Odendaal, "Application of structural winding capacitance cancellation for integrated EMI filters by embedding conductive layers," in *Proc. IEEE Industry Applications Society Annu. Meeting*, Seattle, WA, Oct. 3–7, 2004, pp. 2679–2686.

[7] T. C. Neugebauer, J. W. Phinney, and D. J. Perreault, "Filters and components with inductance cancellation," *IEEE Trans. Ind. Applicat.*, vol. 40, no. 2, pp. 483–491, Mar./Apr. 2004.

[8] T. C. Neugebauer and D. J. Perreault, "Filters with inductance cancellation using printed circuit board transformers," *IEEE Trans. Power Electron.*, vol. 19, no. 3, pp. 591–602, May 2004.

[9] ——, "Parasitic capacitance cancellation in filter inductors," in *Proc. IEEE Power Electronics Specialists Conf.*, Aachen, Germany, Jun. 20–25, 2004, pp. 3102–3107.
[10] EPCOS AG, "Film Capacitor Mannual," Tech. Rep., Munich, Germany, 2000.
[11] R. Anderson, *Test and Measurement Application Note 95-1 S-Parameters Techniques*. Palo Alto, CA: Hewlett-Packard, 1997.
[12] Agilent Technologies, "S-Parameters Design Application Note," Std. Agilent AN154, 2000.

Shuo Wang (S'03) received the B.S.E.E degree from Southwest Jiaotong University, Chengdu, China, in 1994, the M.S.E.E. degree from Zhejiang University, Hangzhou, China, in 1997, and is currently pursuing the Ph.D. degree at the Center for Power Electronics Systems (CPES), Virginia Polytechnic Institute and State University, Blacksburg.

From 1997 to 1999, he was with ZTE Telecommunication Corporation, Shenzhen, China, where he was a Senior R&D Engineer and responsible for the development and support of the power supply for wireless products. In 2000, he worked at UTstarcom Telecommunication Corporation, Hangzhou, where he was responsible for the development and support of the optical access networks. He has one U.S. patent pending

Mr. Wang received the Excellent R&D Engineer Award in 1998.

Fred C. Lee (S'72–M'74–SM'87–F'90) received the B.S. degree in electrical engineering from the National Cheng Kung University, Taiwan, R.O.C., in 1968 and the M.S. and Ph.D. degrees in electrical engineering from Duke University, Durham, NC, in 1971 and 1974, respectively.

He is a University Distinguished Professor with Virginia Polytechnic Institute and State University (Virginia Tech), Blacksburg, and prior to that he was the Lewis A. Hester Chair of Engineering at Virginia Tech. He directs the Center for Power Electronics Systems (CPES), a National Science Foundation engineering research center whose participants include five universities and over 100 corporations. In addition to Virginia Tech, participating CPES universities are the University of Wisconsin-Madison, Rensselaer Polytechnic Institute, North Carolina A&T State University, and the University of Puerto Rico-Mayaguez. He is also the Founder and Director of the Virginia Power Electronics Center (VPEC), one of the largest university-based power electronics research centers in the country. VPEC's Industry-University Partnership Program provides an effective mechanism for technology transfer, and an opportunity for industries to profit from VPEC's research results. VPEC's programs have been able to attract world-renowned faculty and visiting professors to Virginia Tech who, in turn, attract an excellent cadre of undergraduate and graduate students. Total sponsored research funding secured by him over the last 20 years exceeds $35 million. His research interests include high-frequency power conversion, distributed power systems, space power systems, power factor correction techniques, electronics packaging, high-frequency magnetics, device characterization, and modeling and control of converters. He holds 30 U.S. patents, and has published over 175 journal articles in refereed journals and more than 400 technical papers in conference proceedings.

Dr. Lee received the Society of Automotive Engineering's Ralph R. Teeter Education Award (1985), Virginia Tech's Alumni Award for Research Excellence (1990), and its College of Engineering Dean's Award for Excellence in Research (1997), in 1989, the William E. Newell Power Electronics Award, the highest award presented by the IEEE Power Electronics Society for outstanding achievement in the power electronics discipline, the Power Conversion and Intelligent Motion Award for Leadership in Power Electronics Education (1990), the Arthur E. Fury Award for Leadership and Innovation in Advancing Power Electronic Systems Technology (1998), the IEEE Millennium Medal, and honorary professorships from Shanghai University of Technology, Shanghai Railroad and Technology Institute, Nanjing Aeronautical Institute, Zhejiang University, and Tsinghua University. He is an active member in the professional community of power electronics engineers. He chaired the 1995 International Conference on Power Electronics and Drives Systems, which took place in Singapore, and co-chaired the 1994 International Power Electronics and Motion Control Conference, held in Beijing. During 1993-1994, he served as President of the IEEE Power Electronics Society and, before that, as Program Chair and then Conference Chair of IEEE-sponsored power electronics specialist conferences.

Willem Gerhardus Odendaal (M'98) was born in South Africa in 1969. He received the B.Eng., M.Eng., and D.Eng. degrees in electrical and electronics engineering from Rand Arikaans University, Johannesburg, South Africa, in 1992, 1995, and 1997, respectively.

He spent one year in a post-doctoral position under two fellowships at the Virginia Power Electronics Center, Virginia Polytechnic Institute and State University (Virginia Tech), Blacksburg, before joining Philips Research North America, New York, NY, as Senior Member of Research Staff. Since Fall 2001, he has been Assistant Professor in the Bradley Department of Electrical and Computer Engineering, Virginia Tech, as well as a faculty member of the NSF Engineering Research Center for Power Electronics Systems, (or CPES). His research interests include electromagnetic and thermodynamic energy processing and packaging of power electronic circuits.

Dr. Odendaal is Chairman of the Power Electronics Devices and Components Committee, IEEE Industry Applications Society.

Jacobus Daniel van Wyk (F'90) received the M.Sc.Eng. degree from the University of Pretoria, Pretoria, South Africa, in 1966, the Dr.Sc.Tech. degree from the Technical University of Eindhoven, Eindhoven, The Netherlands, in 1969, and the D.Sc. degree (with high honors) in engineering from the University of Natal, Natal, South Africa, in 1996.

He has worked with the S.A. Iron and Steel Corporation, the University of Pretoria, and was a member of the Technical and Scientific Staff, University of Eindhoven, from 1961 to 1971. From 1971 to 1995, he was a Chaired Professor of electrical and electronic engineering at the Rand Afrikaans University, Johannesburg, South Africa, holding Chairs in electronics and in power electronics until 1992. He founded the Industrial Electronics Technology Research Group, Faculty of Engineering, in 1978 and directed this unit until 1999. Since July 1995, he has held a special University Council Research Chair in industrial electronics at the Rand Afrikaans University. He joined The Bradley Department of Electrical and Computer Engineering, Virginia Polytechnic Institute and State University, Blacksburg, in January 2000, where he is the J. Byron Maupin Professor of Engineering, working in the National Science Foundation Engineering Research Center for Power Electronics Systems.

Dr. van Wyk received 20 prize paper awards including 11 IEEE prize paper awards, the prestigious IEEE William E. Newell Power Electronics Award in 1995, an IEEE Third Millennium Medal in 2000, and a range of other awards from IEEE Societies as well as from the South African Institute of Electrical Engineers. He is a Fellow of the South African Institute of Electrical Engineers. He is active in several capacities within the IEEE and its Societies.